
CHALMERS
UNIVERSITY OF TECHNOLOGY

# Robust Snapshot Radio SLAM



Citation for the original published paper (version of record):
Kaltiokallio, O., Rastorgueva-Foi, E., Talvitie, J. et al (2025). Robust Snapshot Radio SLAM. IEEE Transactions on Vehicular Technology, 74(5): 8460-8465.
http://dx.doi.org/10.1109/TVT.2024.3524118



(article starts on next page)

# Robust Snapshot Radio SLAM

Ossi Kaltiokallio, *Member, IEEE*, Elizaveta Rastorgueva-Foi, Jukka Talvitie, *Member, IEEE*, Yu Ge, *Member, IEEE*, Henk Wymeersch, *Fellow, IEEE*, and Mikko Valkama, *Fellow, IEEE*

***Abstract*—The intrinsic geometric connections between millimeter-wave (mmWave) signals and the propagation environment can be leveraged for simultaneous localization and mapping (SLAM) in 5G and beyond networks. However, estimated channel parameters that are mismatched to the utilized geometric model can cause the SLAM solution to degrade. In this paper, we propose a robust snapshot radio SLAM algorithm for mixed line-of-sight (LoS) and non-line-of-sight (NLoS) environments that can estimate the unknown user equipment (UE) state, map of the environment as well as the presence of the LoS path. The proposed method can accurately detect outliers and the LoS path, enabling robust estimation in both LoS and NLoS conditions. The proposed method is validated using 60 GHz experimental data, indicating superior performance compared to the state-of-the-art.**

***Index Terms*—5G, 6G, mmWave, simultaneous localization and mapping, robust estimation.**

## I. Introduction

The development of evolving 5G and future 6G networks provides not only new opportunities for improving the quality and robustness of communications, but also for facilitating high-accuracy localization and sensing [1], [2]. This is enabled by increased temporal and angular resolution due to the use of higher frequency bands and thus larger bandwidths combined with larger antenna arrays. Extracting timely and accurate location and situational awareness is, in general, a critical asset in various applications such as vehicular systems and industrial mobile work machines [3], [4].

Localization and sensing using downlink/uplink signals between the base station (BS) and user equipment (UE) is often a two-stage process [5], in which the channel parameters, that is, the angle-of-arrival (AoA), angle-of-departure (AoD) and time-of-arrival (ToA) of the resolvable propagation paths are first estimated. Then, in the second stage, the channel parameters are used for localization and sensing. The resolvable non-line-of-sight (NLoS) paths provide information not only about the UE position, but also regarding the incidence points of single-bounce NLoS paths. While these incidence points are unknown, the cardinality of the channel parameters can outweigh the unknowns, enabling bistatic radio simultaneous localization and mapping (SLAM) which aims to estimate the unknown UE state and landmark locations using the channel estimates and the known BS state [6]. This is illustrated conceptually in Fig. 1. It is important to note that bistatic radio SLAM makes it possible to estimate the UE state with respect to a global reference system just from single snapshot observation as presented in Section II, whereas conventional SLAM approaches (e.g. based on a camera or LIDAR) typically solve the problem iteratively over time in the local frame of the sensor.

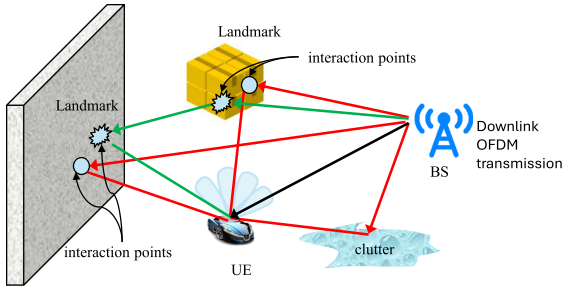


Fig. 1. Illustration of the bistatic snapshot radio SLAM problem where the UE jointly estimates its own state as well as state of the landmarks based on ToA, AoA, and AoD measurements per path. Multi-bounce signals create outlier measurements that have a mismatch to the utilized geometric model.

The bistatic SLAM problem has gained widespread attention in the 5G/6G research field since it improves localization accuracy [5], enables localizing the UE in the absence of line-of-sight (LoS) [7], and reduces the dependence on infrastructure thus enabling localization even with a single BS [6]. To this end, two mainstream approaches exist in literature:

1) *filtering-based solutions* that recursively estimate the joint state of the UE and map by processing the observations sequentially over time;
2) *snapshot approaches* that solve the SLAM problem for a single UE location without any prior information nor kinematic models.

The main benefit of filtering approaches is that higher localization accuracy is expected and state-of-the-art filters [8], [9], [10] can inherently deal with many of the challenges faced in bistatic SLAM including false detections generated by clutter and multi-bounce propagation paths. In contrast, snapshot SLAM is fundamentally important as it serves as a baseline for what can be done with radio signals alone [5], [7], [11], [12] and the solution can be used to initialize and/or as input to filtering approaches. A major limitation of existing snapshot approaches is that they typically overlook outlier measurements that for example originate from multi-bounce propagation paths and that have a mismatch to the utilized geometric model [5], [7], [11], [12]. As a consequence, outliers will cause localization performance degradation.

In this paper, we address the limitations of the state-of-the-art in [5], [7], [11], [12] and develop a novel snapshot SLAM method to estimate the UE state and map of the propagation environment using a single downlink transmission from one BS, that is robust against outlier measurements. The contributions can be summarized as follows:

- We propose a low-complexity processing pipeline for solving the snapshot SLAM problem using measurements that are corrupted by outliers—defined as measurements not originating from LoS or single-bounce NLoS paths;
- In contrast to the methods presented in [7], [11] that always assume NLoS condition when solving the SLAM problem, we present a method to detect the LoS path and solve the problem in mixed LoS/NLoS conditions;
- Using experimental data with off-the-shelf 60 GHz mmWave MIMO radios, we demonstrate that the developed algorithm can

Received 8 July 2024; revised 8 November 2024; accepted 2 December 2024. Date of publication 31 December 2024; date of current version 20 May 2025. This work was supported in part by the Academy of Finland under Grant 338224, Grant 345654, Grant 352754, and Grant 359095, in part by Business Finland6G-ISAC project, and in part by the Vinnova B5GPOS Project under Grant 2022-01640. The review of this article was coordinated by Dr. Hongliang Zhang. *(Corresponding author: Ossi Kaltiokallio.)*

Ossi Kaltiokallio, Elizaveta Rastorgueva-Foi, Jukka Talvitie, and Mikko Valkama are with Tampere University, 33720 Tampere, Finland (e-mail: ossi.kaltiokallio@tuni.fi).

Yu Ge and Henk Wymeersch are with the Chalmers University of Technology, 412 96 Gothenburg, Sweden.

Digital Object Identifier 10.1109/TVT.2024.3524118

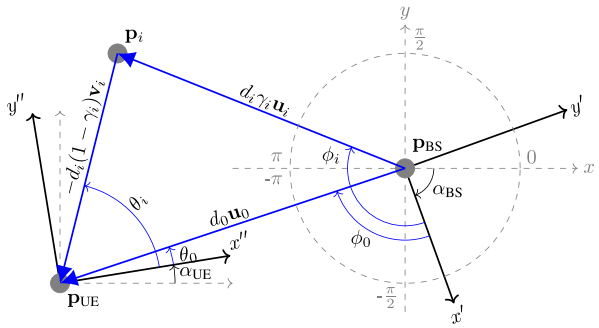


Fig. 2. Problem geometry for an identifiable system with one LoS and one single-bounce NLoS path. The dashed gray axes define the global coordinate system $(x,\ y)$, angles of the propagation paths are expressed in the local frame of the BS $(x',\ y')$ and UE $(x'',\ y'')$ and the notation is introduced in Section III-A2.

accurately recover the inliers resulting in superior accuracy with respect to the state-of-the-art benchmark algorithms.[1]

In this paper, we adopt the following notations. Scalars are denoted in italic (e.g. $x$), vectors in lowercase bold letters (e.g. $\mathbf{x}$), matrices in capital boldface letters (e.g. $\mathbf{X}$) and unordered sets using calligraphic letters (e.g. $\mathcal{X}$). Additionally, $(\cdot)^\top$ and $(\cdot)^{-1}$ denote the transpose and inverse, respectively; $\|\cdot\|$ the Euclidean norm; $|\mathcal{X}|$ cardinality of set $\mathcal{X}$; $\mathbf{I}_n$ the $n\times n$ identity matrix; and $\hat{\mathbf{x}}$ denotes an estimate of $\mathbf{x}$. A multivariate Gaussian distribution with mean $\mathbf{m}$ and covariance $\mathbf{P}$ is denoted as $\mathcal{N}(\mathbf{m},\mathbf{P})$.

## II. Problem Formulation and Models

Considering the experimental setup in Section IV and to simplify the presentation, we focus on describing the methods in the 2D/azimuth domain but extension to 3D is possible (conceptually similar to, e.g., [7]). The BS state is represented by the position $\mathbf{p}_{\text{BS}}\in\mathbb{R}^2$ and orientation $\alpha_{\text{BS}}\in[-\pi,\pi]$. The $i$th landmark is represented by position $\mathbf{p}_i\in\mathbb{R}^2$ which depicts the interaction point of the $i$th single-bounce propagation path. The UE state, $\mathbf{x}$, is described using the position $\mathbf{p}_{\text{UE}}\in\mathbb{R}^2$, orientation $\alpha_{\text{UE}}$ and clock bias $b_{\text{UE}}$, that is, the difference between the BS and UE clocks.

### A. System Model

The problem geometry is illustrated in Fig. 2, considering the BS as transmitter and the UE as receiver. The BS and UE are equipped with antenna arrays and we consider beam-based orthogonal frequency-division multiplexing (OFDM) transmission utilizing beam sweeping at both the BS and UE. Assuming coarse timing information for obtaining OFDM symbols within an applicable time window, under which the channel is assumed constant, the received sample of the $l$th OFDM-symbol and $k$th subcarrier with $m$th BS beam and $n$th UE beam can be described as [13]

$$y_{k,l}^{m,n}=\sum_{i=0}^{N}\xi_i G_{\text{BS}}^{m}(\phi_i)G_{\text{UE}}^{n}(\theta_i)e^{-\text{j}2\pi k\Delta f\tau_i}x_{k,l}^{m,n}+w_{k,l}^{m,n},\quad(1)$$

where $\Delta f$ is the subcarrier spacing and $w_{k,l}^{m,n}$ denotes noise after applying the UE beam. In addition, $\xi_i$, $\tau_i$, $\phi_i$, $\theta_i$ are the complex path coefficient, ToA, AoD, and AoA for the $i$th propagation path, respectively. Element $i=0$ is reserved for the LoS path (if such is present and detected) and $N$ is the number of NLoS propagation paths. To distinguish between these cases, let the hypothesis $\mathcal{H}=\mathcal{H}_0$ represent the LoS condition, while the alternate hypothesis $\mathcal{H}=\mathcal{H}_1$ represents the NLoS condition. Furthermore, $G_{\text{BS}}^{m}(\phi_i)\in\mathbb{C}$ and $G_{\text{UE}}^{n}(\theta_i)\in\mathbb{C}$ are angular responses, containing effects of steering vectors and beamformers,[2] for the $m$th BS beam and $n$th UE beam in respective order. Depending on the knowledge of $G_{\text{BS}}^{m}(\phi_i)$ and $G_{\text{UE}}^{n}(\theta_i)$, various methods for estimating the channel parameters exist [5], [13], [14].

### B. Geometric Measurement Model

Let $\mathbf{z}_i=[\tau_i,\ \phi_i,\ \theta_i]^\top$ denote the channel parameter estimate of the $i$th propagation path, referred to as 'measurement' from now on and let $\mathcal{Z}$ and $\mathcal{I}$ denote a set of measurements and associated indices, respectively. Assuming that the measurement noise is zero-mean Gaussian, which is a common assumption in SLAM [9], the likelihood function is Gaussian

$$p(\mathbf{z}_i\mid\mathbf{x},\mathbf{p}_i)=\mathcal{N}(\mathbf{z}_i\mid\mathbf{h}(\mathbf{x},\mathbf{p}_i),\mathbf{\Sigma}_i),\quad(2)$$

with mean $\mathbf{h}_i(\mathbf{x},\mathbf{p}_i)$ and diagonal covariance matrix $\mathbf{\Sigma}_i=\text{diag}([\sigma_{\tau_i}^2,\ \sigma_{\phi_i}^2,\ \sigma_{\theta_i}^2])$ in which $\sigma_{\tau_i}^2$, $\sigma_{\phi_i}^2$ and $\sigma_{\theta_i}^2$ denote variance of the ToA, AoD and AoA, respectively. Building on the geometry in Fig. 2, the mean of LoS and single-bounce NLoS paths is given by

$$\mathbf{h}(\mathbf{x},\mathbf{p}_i)=\begin{bmatrix}t_i+b_{\text{UE}}\\ \text{atan2}(-\delta_{i,1,y},-\delta_{i,1,x})-\alpha_{\text{BS}}\\ \text{atan2}(\delta_{i,2,y},\delta_{i,2,x})-\alpha_{\text{UE}}\end{bmatrix}\quad(3)$$

and it represents the geometric relationship between the BS, UE and landmark. The parameters are defined as:

- LoS path $(i=0)$: $\mathbf{p}_0=\emptyset$, $t_0=\|\mathbf{p}_{\text{BS}}-\mathbf{p}_{\text{UE}}\|/c$ in which $c$ denotes the speed of light and $[\delta_{0,1,x},\ \delta_{0,1,y}]^\top=[\delta_{0,2,x},\ \delta_{0,2,y}]^\top=\mathbf{p}_{\text{BS}}-\mathbf{p}_{\text{UE}}$.
- NLoS path $(i\neq 0)$: $t_i=\|\mathbf{p}_{\text{BS}}-\mathbf{p}_i\|/c+\|\mathbf{p}_i-\mathbf{p}_{\text{UE}}\|/c$, $[\delta_{i,1,x},\ \delta_{i,1,y}]^\top=\mathbf{p}_{\text{BS}}-\mathbf{p}_i$ and $[\delta_{i,2,x},\ \delta_{i,2,y}]^\top=\mathbf{p}_i-\mathbf{p}_{\text{UE}}$.

## III. Snapshot SLAM

The procedure to solve the SLAM problem depends on $\mathcal{H}$. We first solve the problem considering $\mathcal{H}$ to be known and then generalize the method to detect the LoS existence in Section III-C. Moreover, we first assume measurements without outliers in Section III-A while this assumption is relaxed in Section III-B.

### A. Snapshot SLAM Without Outliers

*1) Orientation Estimate:* The procedure to determine the orientation for both $\mathcal{H}_0$ and $\mathcal{H}_1$ is described in the following.

i) *LoS condition $\mathcal{H}_0$* – From Fig. 2, we see immediately that the UE orientation is given by

$$\hat{\alpha}_{\text{UE}}=\text{atan2}(y,x),\quad(4)$$

where $[x,\ y]^\top=-\mathbf{R}(-\theta_0)\mathbf{u}_0$. Hence, the UE positioning problem is solved by first estimating $\hat{\alpha}_{\text{UE}}$ using (4) and thereafter, the conditional position and clock bias estimate, $\hat{\mathbf{x}}_{\alpha_{\text{UE}}}=[\hat{\mathbf{p}}_{\text{UE}}^\top,\ \hat{b}_{\text{UE}}]^\top$, is computed as described in Section III-A2.

[1] We provide the channel estimates for the experimental data as well as Matlab code for the presented algorithms, both available at: https://github.com/okaltiok/Robust-snapshot-radio-SLAM

[2] More concretely, for example $G_{\text{BS}}^{m}(\phi)=\mathbf{a}_{\text{BS}}^\top(\phi)\mathbf{f}_m$, for BS steering vector $\mathbf{a}_{\text{BS}}^\top(\phi)$ and beamformer $\mathbf{f}_m$.

ii) *NLoS condition* $\mathcal{H}_1$ – The problem does not admit a closed-form solution and we must resort to numerical optimization methods as in [7] to obtain the state estimate. The optimization problem is defined as

$$\hat{\alpha}_{\text{UE}} = \arg\min_{\alpha_{\text{UE}} \in \mathcal{A}} J(\hat{\mathbf{x}}_{\alpha_{\text{UE}}}), \tag{5}$$

where $\mathcal{A}$ denotes a grid of possible UE orientations, $J(\hat{\mathbf{x}}_{\alpha_{\text{UE}}})$ is the cost given in (13) in which $\hat{\mathbf{x}}_{\alpha_{\text{UE}}}$ is computed using (15).

*2) Conditional Position and Clock Bias Estimate:* Let $\mathbf{x}_{\alpha_{\text{UE}}} = [\mathbf{p}_{\text{UE}}^\top, b_{\text{UE}}]^\top$ denote the partial UE state given $\alpha_{\text{UE}}$. As illustrated in Fig. 2, the AoD and AoA for a single path can be represented by unit vectors $\mathbf{u}_i$ and $\mathbf{v}_i$, given by

$$\mathbf{u}_i = \mathbf{R}(\alpha_{\text{BS}}) \begin{bmatrix} \cos(\phi_i) & \sin(\phi_i) \end{bmatrix}^\top, \tag{6}$$

$$\mathbf{v}_i = \mathbf{R}(\alpha_{\text{UE}}) \begin{bmatrix} \cos(\theta_i) & \sin(\theta_i) \end{bmatrix}^\top, \tag{7}$$

in which $\mathbf{R}(\alpha)$ is a counterclockwise rotation matrix, defined as

$$\mathbf{R}(\alpha) = \begin{bmatrix} \cos(\alpha) & -\sin(\alpha) \\ \sin(\alpha) & \cos(\alpha) \end{bmatrix}. \tag{8}$$

Using $\mathbf{u}_i$ and $\mathbf{v}_i$, the UE position is given by [7]:

$$\mathbf{p}_{\text{UE}} = \mathbf{p}_{\text{BS}} + d_i \gamma_i \mathbf{u}_i - d_i(1-\gamma_i)\mathbf{v}_i \tag{9}$$

where $d_i = c(\tau_i - b_{\text{UE}})$ denotes the propagation distance and $\gamma_i \in [0,1]$ is unknown and represents the fraction of the propagation distance along $\mathbf{u}_i$.

The position and clock bias can be estimated utilizing the geometric relationship defined in (9) as follows. First, the expression in (9) can be rearranged as follows

$$\mathbf{H}_i \mathbf{x}_{\alpha_{\text{UE}}} = \boldsymbol{\mu}_i + \gamma_i d_i \boldsymbol{\nu}_i \tag{10}$$

where $\mathbf{H}_i = [\mathbf{I}_2, -c\mathbf{v}_i]$, $\boldsymbol{\mu}_i = \mathbf{p}_{\text{BS}} - c\tau_i \mathbf{v}_i$ and $\boldsymbol{\nu}_i = \mathbf{u}_i + \mathbf{v}_i$. Then, we solve for $\gamma_i$ through

$$\gamma_i = \boldsymbol{\nu}_i^\top (\mathbf{H}_i \mathbf{x}_{\alpha_{\text{UE}}} - \boldsymbol{\mu}_i)/(d_i \boldsymbol{\nu}_i^\top \boldsymbol{\nu}_i) \tag{11}$$

and substitute it back to (10) which yields

$$\mathbf{H}_i \mathbf{x}_{\alpha_{\text{UE}}} = \boldsymbol{\mu}_i + \bar{\boldsymbol{\nu}}_i^\top (\mathbf{H}_i \mathbf{x}_{\alpha_{\text{UE}}} - \boldsymbol{\mu}_i)\bar{\boldsymbol{\nu}}_i, \tag{12}$$

where $\bar{\boldsymbol{\nu}}_i = \boldsymbol{\nu}_i / \|\boldsymbol{\nu}_i\|$. Now, considering all the paths gives the following cost function [11]

$$J(\mathbf{x}_{\alpha_{\text{UE}}}) = \sum_{i \in \mathcal{I}} \eta_i J_i(\mathbf{x}_{\alpha_{\text{UE}}}), \quad \text{where} \tag{13}$$

$$J_i(\mathbf{x}_{\alpha_{\text{UE}}}) = \|\mathbf{H}_i \mathbf{x}_{\alpha_{\text{UE}}} - \boldsymbol{\mu}_i - \bar{\boldsymbol{\nu}}_i^\top (\mathbf{H}_i \mathbf{x}_{\alpha_{\text{UE}}} - \boldsymbol{\mu}_i)\bar{\boldsymbol{\nu}}_i\|^2 \tag{14}$$

and $\eta_i = |\hat{\xi}_i|^2$ in which $\hat{\xi}_i$ denotes the complex path coefficient estimate. Lastly, a closed-form solution can be obtained by setting the gradient of (13) to zero and solving for $\mathbf{x}_{\alpha_{\text{UE}}}$ [11]

$$\hat{\mathbf{x}}_{\alpha_{\text{UE}}} = \left( \sum_{i \in \mathcal{I}} \mathbf{A}_i \right)^{-1} \sum_{i \in \mathcal{I}} \mathbf{b}_i, \tag{15}$$

in which $\mathbf{A}_i = \eta_i \mathbf{H}_i^\top (\mathbf{I}_2 - \bar{\boldsymbol{\nu}}_i \bar{\boldsymbol{\nu}}_i^\top)\mathbf{H}_i$, $\mathbf{b}_i = \eta_i \mathbf{H}_i^\top (\mathbf{I}_2 - \bar{\boldsymbol{\nu}}_i \bar{\boldsymbol{\nu}}_i^\top)\boldsymbol{\mu}_i$ and the complete state estimate is denoted as $\hat{\mathbf{x}} = [\hat{\mathbf{p}}_{\text{UE}}^\top, \hat{\alpha}_{\text{UE}}, \hat{b}_{\text{UE}}]^\top$. The SLAM problem is identifiable and all unknowns can be estimated if a sufficient number of NLoS paths exist since each NLoS path provides three measurements, while being parameterized by two unknowns (i.e., $\mathbf{p}_i$). With known clock bias either the LoS or three NLoS are required [15], whereas one NLoS and the LoS ($N_{\min} = 2$) or four NLoS ($N_{\min} = 4$) are needed if the BS and UE are not synchronized. Fig. 2 illustrates the problem geometry for an identifiable system with a minimum number of paths and it is important to note that for the LoS path ($i = 0$), we have $\mathbf{v}_0 = -\mathbf{u}_0$, $\bar{\boldsymbol{\nu}}_0 = \mathbf{0}$ and $\gamma_0 = 1$.

*3) Landmark Estimate:* Given $\hat{\mathbf{x}}$, the landmark locations can be estimated by solving a nonlinear optimization problem for every NLoS propagation path $i = 1, 2, \ldots, N$, independently. The optimization problem is defined as

$$\hat{\mathbf{p}}_i = \arg\min_{\mathbf{p}_i} (\mathbf{z}_i - \mathbf{h}(\mathbf{x}, \mathbf{p}_i))^\top \boldsymbol{\Sigma}_i^{-1} (\mathbf{z}_i - \mathbf{h}(\mathbf{x}, \mathbf{p}_i)), \tag{16}$$

where $\mathbf{h}(\mathbf{x}, \mathbf{p}_i)$ and $\boldsymbol{\Sigma}_i$ are given in (2). The optimization problem can be solved using the Gauss-Newton algorithm [16] which is initialized using $\mathbf{p}_i = (\mathbf{p}_{\text{BS},i} + \mathbf{p}_{\text{UE},i})/2$ where $\mathbf{p}_{\text{BS},i}$ and $\mathbf{p}_{\text{UE},i}$ are vectors that span towards $\mathbf{p}_i$ from the BS, $\mathbf{p}_{\text{BS},i} = \mathbf{p}_{\text{BS}} + \hat{d}_i \hat{\gamma}_i \hat{\mathbf{u}}_i$ and UE, $\mathbf{p}_{\text{UE},i} = \hat{\mathbf{p}}_{\text{UE}} + \hat{d}_i(1-\hat{\gamma}_i)\hat{\mathbf{v}}_i$, respectively, and parameters $\hat{\mathbf{u}}_i$, $\hat{\mathbf{v}}_i$, $\hat{d}_i$ and $\hat{\gamma}_i$ are computed by plugging $\hat{\mathbf{x}}$ into (6), (7) and (10).

## B. Robust Snapshot SLAM

The SLAM algorithm described in the previous section is sensitive to measurement outliers. In the worst case, measurements that cannot be expressed using (9) cause the solution to be very inaccurate. In the following, a robust SLAM approach which is inspired by the random sample consensus (RANSAC) algorithm [17] is described. The aim of the robust SLAM algorithm is to find a subset of $\mathcal{Z}$ that does not contain outliers and which is then used to estimate $\hat{\mathbf{x}}$. Instead of randomly sampling subsets of $\mathcal{Z}$ as in RANSAC to determine $\hat{\mathbf{x}}$, we can perform an exhaustive search over all possible combinations instead, since $|\mathcal{Z}|$ is typically quite low. In the experimental setup considered in Section IV, the number of measurements ranged from 4 to 11 [13] and an exhaustive search is feasible since the number of possible combinations is at most 330. The number of measurements is inline with the indoor 60 GHz channel measurements conducted in [18] which reported that the number of identified clusters ranged from 6 to 12 in LoS conditions and from 8 to 12 in NLoS conditions. Furthermore, methods to reduce the search space exist and potential alternatives are discussed in Section IV.

Let, with a slight abuse of notation, $\mathcal{I}_{\text{all}}$ denote the set of indices of $\mathcal{Z}$. Furthermore, let $\mathcal{P}(\mathcal{I}_{\text{all}})$ denote the power set of $\mathcal{I}_{\text{all}}$, that is, the set of all subsets of $\mathcal{I}_{\text{all}}$. In the context of RANSAC, minimal solvers that compute solutions from a minimal amount of data, $N_{\min}$ in our case, are preferable because it increases the likelihood of using a set that has no outliers. In other words, RANSAC utilizes $\mathcal{J} \in \mathcal{P}(\mathcal{I}_{\text{all}})$ for which $|\mathcal{J}| = N_{\min}$. In this paper on the other hand, we perform an exhaustive search over all such subsets and in the LoS condition one of the elements of $\mathcal{J}$ is always $i = 0$.[3] Overall, there are $L$ combinations

$$L \triangleq |\mathcal{J}| = \frac{(|\mathcal{Z}| - N_{\text{LoS}})!}{(|\mathcal{Z}| - N_{\text{LoS}} - N_{\text{NLoS}})!\, N_{\text{NLoS}}!}, \tag{17}$$

in which $N_{\text{LoS}}$ and $N_{\text{NLoS}}$ denote the minimum number of LoS and NLoS paths required to solve the SLAM problem.

The robust snapshot SLAM problem is defined as follows. For each set $\mathcal{I} \in \mathcal{J}$ and each value of $\alpha_{\text{UE}} \in \mathcal{A}$ (under $\mathcal{H}_1$), the corresponding cost is $\sum_{i \in \mathcal{I}} \eta_i J_i(\hat{\mathbf{x}}_{\alpha_{\text{UE}}})$. According to the principles of RANSAC, from the solution $\hat{\mathbf{x}}_{\alpha_{\text{UE}}}$ and using an inlier detection threshold $T_\varepsilon$, the measurements are partitioned into a set of inliers and a set of outliers. A final cost is then computed, denoted by $C(\alpha_{\text{UE}}, \mathcal{I}) = C_{\text{inlier}}(\alpha_{\text{UE}}, \mathcal{I}) +$

[3] Example for $|\mathcal{Z}| = 4$:
1) *LoS condition* $\mathcal{H}_0$: $\mathcal{I}_{\text{all}} = \{0,1,2,3\}$, $N_{\min} = 2$, $N_{\text{LoS}} = 1$, $N_{\text{NLoS}} = 1$, $L = 3$ and $\mathcal{J} = \{\{0,1\}, \{0,2\}, \{0,3\}\}$;
2) *NLoS condition* $\mathcal{H}_1$: $\mathcal{I}_{\text{all}} = \{1,2,3,4\}$, $N_{\min} = 4$, $N_{\text{LoS}} = 0$, $N_{\text{NLoS}} = 4$, $L = 1$ and $\mathcal{J} = \{1,2,3,4\}$.
To note, $\mathcal{I}$ in Section III-A corresponds to $\mathcal{I}_{\text{all}}$.

**Algorithm 1:** Robust Snapshot SLAM Algorithm.

**In:** Combinations $\mathcal{J}$, LoS/NLoS condition $\mathcal{H}$, $M$, $\mathcal{Z}$
**Out:** Cost matrix $\mathbf{C} \in \mathbb{R}^{L\times|\mathcal{A}|}$
**if** $\mathcal{H}=\mathcal{H}_0$ **then** $\mathcal{A}=\{0\}$ **else** $\mathcal{A}=\text{linspace}(-\pi,\pi,M)$
**for** $m=1:|\mathcal{A}|$ **do**
  **for** $l=1:L$ **do**
    **if** $\mathcal{H}=\mathcal{H}_0$ **then** $\alpha_{\text{UE}} \leftarrow$ (4) **else** $\alpha_{\text{UE}} \leftarrow \{\mathcal{A}\}_m$
    Set $C_{l,m}=\infty$
    Set $\mathcal{I} \leftarrow \{\mathcal{J}\}_l$ and compute $\hat{\mathbf{x}}_{\alpha_{\text{UE}}}$ using (15) based on $\mathcal{I}$
    Set $\mathcal{I}_{\text{inliers}}=\{i\in\mathcal{I}_{\text{all}} \mid J_i(\hat{\mathbf{x}}_{\alpha_{\text{UE}}}) \le T_\varepsilon\}$
    Set $\mathcal{I}_{\text{outliers}}=\mathcal{I}_{\text{all}}\setminus\mathcal{I}_{\text{inliers}}$
    Recompute $\hat{\mathbf{x}}_{\alpha_{\text{UE}}}$ using (15) based on $\mathcal{I}_{\text{inliers}}$
    **if** `is_feasible`$(\hat{\mathbf{x}}_{\alpha_{\text{UE}}},\mathcal{I}_{\text{inliers}},\mathcal{Z})$ **then**

$$C_{l,m}=\underbrace{\sum_{i\in\mathcal{I}_{\text{inliers}}}\eta_i J_i(\hat{\mathbf{x}}_{\alpha_{\text{UE}}})}_{C_{\text{inlier}}}+\underbrace{\sum_{i\in\mathcal{I}_{\text{outliers}}}\eta_i T_\varepsilon}_{C_{\text{outlier}}} \tag{18}$$

**function** `is_feasible`$(\mathbf{x}_{\alpha_{\text{UE}}},\mathcal{I},\mathcal{Z})$

$j=\arg\min_{i\in\mathcal{I}}\{\tau_i\}$
**if** $|\mathcal{I}|<N_{\min}$, **return false** (19a)
**if** $\tau_j - b_{\text{UE}}<0$, **return false** (19b)
**if** $\neg(0\le\gamma_i\le 1 \vee \|\boldsymbol{\nu}_j\|^2 \le T_{\boldsymbol{\nu}})$, **return false** (19c)
**if** $\neg(0\le\gamma_i\le 1),\quad i\in\mathcal{I}\setminus\{j\}$, **return false** (19d)
**return true**

$C_{\text{outlier}}(\alpha_{\text{UE}},\mathcal{I})$. The penalty $C_{\text{outlier}}(\alpha_{\text{UE}},\mathcal{I})$ is added to ensure that the solution favors estimates obtained with as many inliers as possible. Finally, the optimal solution is found as $\arg\min_{\alpha_{\text{UE}},\mathcal{I}} C(\alpha_{\text{UE}},\mathcal{I})$. The complete method is detailed in Algorithm 1, including the computation of the inlier and outlier cost, as well as the search over minimal index sets $\mathcal{I}$ (indexed by $l$) and UE orientations $\alpha_{\text{UE}}$ (indexed by $m$).

To ensure that the solution is physically meaningful, fundamental feasibility constraints are verified for each solution, given in (19). First, the number of inliers should be sufficient to compute $\hat{\mathbf{x}}_{\alpha_{\text{UE}}}$ as stated in (19a). Second, the unbiased delay of the shortest path has to be positive as given in (19b). Third, either the shortest path has to follow (9) or unit vectors of the shortest path must be opposite and nearly parallel as given in (19c) in which $T_{\boldsymbol{\nu}}$ is a threshold. Fourth, the constraint in (19d) comes from the definition of $\mathbf{p}_{\text{UE}}$ in (9).

### C. Extension to LoS Detection and Mixed LoS/NLoS

Thus far, $\mathcal{H}$ has been assumed known and in the following, the proposed robust snapshot SLAM algorithm is generalized to detect $\mathcal{H}_0$ and solve the problem in mixed LOS/NLoS conditions. In this paper, the SLAM problem is solved in mixed LoS/NLoS conditions by first assuming that $\mathcal{H}_0$ is true and using a candidate LoS path. Thereafter, a statistical test is performed to validate the obtained solution and if the validation test fails, the SLAM problem is solved again assuming $\mathcal{H}_1$. It is to be noted that assuming $\mathcal{H}_1$ is always possible, but may lead to performance degradation under $\mathcal{H}_0$ as presented in Section IV-B3. Various well-known LoS detection methods from literature were tried but they were either not directly applicable to the considered problem (e.g., [19]) or the performance was unsatisfactory due to the differences in the considered radio channels (e.g., [20]).

First of all, the LoS candidate is the path with smallest delay, $j=\arg\min_{i\in\mathcal{I}_{\text{all}}}\{\tau_i\}$, after which the estimate $\hat{\mathbf{x}}$ is obtained using Algorithm 1. Second, we model the LoS signal strength in decibels, $\eta_j^{\text{dB}}=10\log_{10}(\eta_j)$, using the log-distance path loss model [21]:

$$\eta_j^{\text{dB}} \sim \mathcal{N}(f(\mathbf{p}_{\text{UE}}),\sigma^2), \tag{20}$$

where $f(\mathbf{p}_{\text{UE}})=L_0+10\zeta\log_{10}(\|\mathbf{p}_{\text{BS}}-\mathbf{p}_{\text{UE}}\|)$, $L_0$ is the reference path loss at a distance of one meter and $\zeta$ is the path loss coefficient. The model parameters $(L_0,\zeta,\sigma^2)$ can be learned from training data or derived from existing models (see e.g. [21, Table III]). Third, the utilized statistical test is based on the negative log-likelihood of $\eta_j^{\text{dB}}$:

$$\frac{1}{2}\left(\log(2\pi\sigma^2)+\frac{1}{\sigma^2}\left(\eta_j^{\text{dB}}-f(\hat{\mathbf{p}}_{\text{UE}})\right)^2\right)\underset{\mathcal{H}_0}{\overset{\mathcal{H}_1}{\gtrless}} T_{\text{LoS}}. \tag{21}$$

If $\mathcal{H}_0$ is false, the SLAM problem is re-solved assuming $\mathcal{H}_1$.

## IV. Experimental Results

### A. Experimental Data and Assumptions

The performance of the proposed and benchmark SLAM algorithms is evaluated using real-world 60 GHz measurement data, obtained indoors at Tampere University campus, with floorplan as illustrated in Fig. 3. Altogether 45 UE locations were measured—32 in LoS and 13 in NLoS conditions. Beamformed measurements were obtained using 400 MHz transmission bandwidth utilizing 5G NR-specified downlink positioning reference signals. The details of the experimental setup and hardware are given in [22]. In this paper, the AoDs and AoAs are estimated from the beam reference signal received power measurements using a singular value decomposition (SVD)-based detector and thereafter, the pathwise ToAs are estimated in frequency domain as presented in [13]. Nearly 30% of the detected propagation paths are multi-bounce signals which will cause SLAM performance degradation if not handled properly.

The proposed SLAM algorithm utilizes the following parameters in the evaluations. In NLoS conditions, 1° angle resolution ($|\mathcal{A}|=361$) is used. We utilize the path loss coefficient, $\zeta=1.7$, and standard deviation, $\sigma=1.8$ dB, of the generic 60GHz path loss model [21, Table III] and $L_0=13$ dB is calibrated from experimental data. The LoS detection threshold in (21) is $T_{\text{LoS}}=10.8$ which is computed using the inverse cumulative distribution function of the $\chi^2$ distribution with tail probability 0.001. The inlier detection threshold used in Algorithm 1 is $T_\varepsilon=0.1$ and the constraint threshold in (19c) is $T_{\boldsymbol{\nu}}=0.1$. The covariance matrix in (16) is empirically tuned and the used value is $\boldsymbol{\Sigma}_i=\text{diag}([1\text{ ns}^2,\ 1\text{ deg}^2,\ 1\text{ deg}^2])$, $\forall i$. However, it is important to note that the UE estimate does not depend on $\boldsymbol{\Sigma}_i$ and the covariance matrix only impacts the landmark estimates via the Gauss-Newton algorithm.

The proposed robust snapshot SLAM algorithm is benchmarked with respect to a method that combines features of the estimators introduced in [7], [11]. The benchmark method estimates the UE position and clock bias in closed-form using the method presented in [11] and the UE orientation is solved using the numerical optimization method presented in [7]. The implemented benchmark algorithm is computationally more efficient than [7] which relies on numerical optimization to solve both the UE orientation and clock bias. In addition, the implemented benchmark algorithm can estimate the unknown UE orientation, whereas the method proposed in [11] assumes the orientation is known. Similar to the methods in [7], [11], the implemented benchmark algorithm always assumes $\mathcal{H}_1$.

### B. Results

*1) Qualitative Comparison:* The solution in one example measurement position is illustrated in Fig. 3(a) using the proposed robust

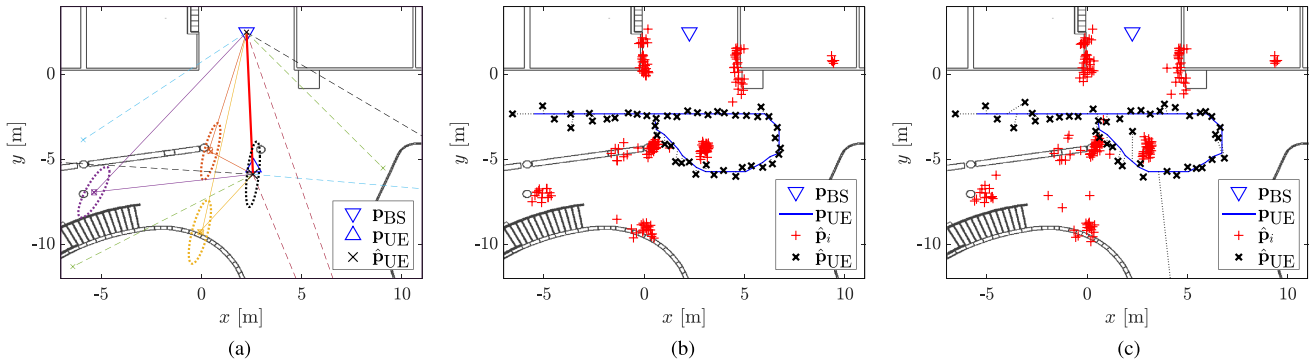


Fig. 3. Example SLAM performance using the proposed and benchmark methods. In (a), the obtained snapshot SLAM solution using the proposed method in one measurement position. In the figure, LoS path illustrated using (——), single-bounce NLoS paths with solid lines, propagation paths that are identified as outliers shown using dashed lines (plotted by plugging $\gamma_i = 0.5$ in to the single-bounce model in (9)) and the dotted ellipses illustrate the one standard deviation uncertainty ellipse of the UE and landmark position estimates. In (b) and (c), $\hat{\mathbf{p}}_{\text{UE}}$ and $\hat{\mathbf{p}}_i$'s for all 45 measurement positions are shown. (a) Example solution. (b) Proposed method. (c) Benchmark method w/o outliers [7], [11].

TABLE I
RMSEs AND CPU TIME OF THE PROPOSED AND BENCHMARK METHODS WITH AND WITHOUT OUTLIERS

| Method | Pos. [m] | Head. [deg] | Clk. [ns] | Time [ms] |
|---|---|---|---|---|
| Proposed | **0.36** | **2.05** | **1.45** | 2.86 |
| Benchmark | 11.11 | 83.79 | 46.52 | **0.91** |
| Proposed* | **0.36** | **2.05** | **1.45** | **0.49** |
| Benchmark* | 1.40 | 4.06 | 4.73 | 0.70 |

*data w/o outliers.

TABLE II
RMSEs AND CPU TIME OF THE PROPOSED METHOD AND BENCHMARK METHOD WITHOUT OUTLIERS IN LOS AND NLOS CONDITIONS

| Method | Pos. [m] | Head. [deg] | Clk. [ns] | Time [ms] |
|---|---|---|---|---|
| Proposed (LoS) | **0.29** | **1.95** | **1.06** | **0.02** |
| Benchmark (LoS) | 1.63 | 4.61 | 5.43 | 0.71 |
| Proposed (NLoS) | **0.49** | 2.27 | **2.13** | 9.85 |
| Benchmark (NLoS) | 0.51 | **2.13** | 2.18 | **0.68** |

snapshot SLAM algorithm. In the example, the proposed method can correctly resolve the LoS and single-bounce NLoS paths leading to an accurate SLAM solution in which the UE position estimate is close to the ground truth and the landmark position estimates closely align with the floor plan of the experimental environment. As illustrated in the figure, the propagation paths that are identified as outliers correspond to three double-bounce propagation paths and one triple-bounce propagation path (dashed green line). In all 45 measurements positions, the proposed method can accurately identify the propagation paths that are inline with the model in (9) leading to good SLAM performance as illustrated in Fig. 3(b). Overall, the utilized channel estimator detects 362 propagation paths and the proposed algorithm classifies 104 of the paths as outliers. Since the benchmark method cannot inherently deal with outliers, they are removed from the data.[4] The SLAM performance for the benchmark method is illustrated in Fig. 3(c) and as shown, the method is clearly not as accurate even without outliers.

*2) Quantitative Comparison:* Since the ground truth landmark locations are unknown, which is a common problem in SLAM when using real-world experimental data, the quantitative evaluation focuses on the UE state. The position, heading and clock bias root mean squared errors (RMSEs) are tabulated in Table I, and the performance is summarized both with and without outliers. The benchmark method yields poor performance with outliers and the accuracy improves notably without outliers. The proposed method yields equivalent SLAM accuracy in both cases and the results demonstrate that the presented outlier removal method is effective in practice. In Table II, the RMSEs are reported separately in the LoS (32/45 UE locations) and NLoS (13/45 UE locations) conditions. The proposed method and benchmark method without outliers yield comparative performance in NLoS conditions and the small difference between the two is due to the different outlier removal methods. In LoS conditions, the proposed method yields superior accuracy since the method explicitly exploits constraints of the LoS signal, whereas the benchmark method does not since it always assumes $\mathcal{H}_1$ and treats the LoS as any single-bounce path. The benefits of utilizing the LoS are further discussed in the next section.

[4]Using the ground truth UE state $\mathbf{x}$ and outlier threshold $T_{\text{outlier}} = 3$, $\mathbf{z}_i$ is labeled an outlier if, $(\mathbf{z}_i - \mathbf{h}(\mathbf{x}, \hat{\mathbf{p}}_i))^\top \mathbf{\Sigma}_i^{-1} (\mathbf{z}_i - \mathbf{h}(\mathbf{x}, \hat{\mathbf{p}}_i)) > T_{\text{outlier}}$, in which $\hat{\mathbf{p}}_i$ is computed using (16).

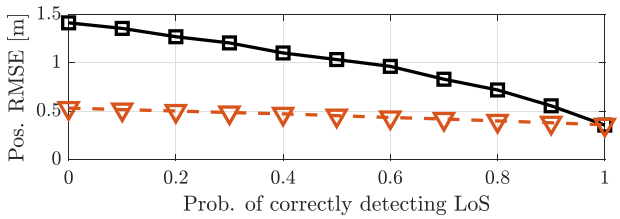


Fig. 4. Position RMSE as a function of $P(\mathcal{H}_0|\text{LoS})$ and the legend is defined as: RMSE for all 45 measurement positions (—□—) and RMSE computed without $\mathbf{p}_{\text{UE}} = [3.56, -5.70]^\top$ (- -▽- -).

*3) LoS Detection Accuracy:* In the considered experimental setting, the LoS detection routine presented in Section III-C yields perfect detection accuracy, $P(\mathcal{H}_0|\text{LoS}) = 1$ and $P(\mathcal{H}_1|\text{NLoS}) = 1$, but it is to be noted that perfect accuracy is not mandatory. To further investigate SLAM performance with an imperfect LoS detector, we synthetically vary the probability of correctly detecting the LoS, $P(\mathcal{H}_0|\text{LoS}) \in [0, 1]$, and perform 1000 Monte Carlo simulations with each value of $P(\mathcal{H}_0|\text{LoS})$. The result is illustrated in Fig. 4. Since the estimate at $\mathbf{p}_{\text{UE}} = [3.56, -5.70]^\top$ happens to be very inaccurate if the LoS is misdetected, the RMSE is computed with and without this unfavorable position. Interestingly when $P(\mathcal{H}_0|\text{LoS}) = 0$, the problem is solved assuming NLoS only and the performance is equivalent to the benchmark method without outliers, indicating the proposed method

is robust to outliers even without the LoS detector. Furthermore, as $P(\mathcal{H}_0|\text{LoS})$ increases, the RMSE decreases which suggests that it is beneficial to solve the problem using the LoS if it exists. The main benefit of using the LoS is that the AoDs and AoAs define the entire geometry up to a scaling since the UE orientation is solved in closed-form and the scaling is determined by the clock bias. In addition, the number of degrees of freedom is lower. Thus, the problem is easier to solve and identifiability of the model is improved leading to increased robustness and enhanced SLAM accuracy when constraints imposed by the LoS are exploited.

*4) Computational Complexity:* The computational complexity of the algorithms are given in the last column of Tables I and II, obtained using a Lenovo ThinkPad P1 Gen 2 with a 2.6 GHz Intel i7-9850H CPU and 64 GB of memory. A naive implementation of the proposed and benchmark algorithms scale according to $\mathcal{O}(|\mathcal{A}| \times L)$ and $\mathcal{O}(|\mathcal{A}|)$, respectively. Solving the SLAM problem in LoS conditions using the proposed method is very efficient since $|\mathcal{A}| = 1$ and $L = |\mathcal{Z}| - 1$. On the other hand, solving the problem is up to three orders of magnitude higher in NLoS conditions since $|\mathcal{A}| = 361$ and typically $L$ is much larger. With respect to the benchmark method, the computational complexity of the proposed method is lower/higher in LoS/NLoS condition and real-time operation with both methods can be easily guaranteed using for example a Matlab MEX-implementations as tabulated in the tables.

In general, there exists numerous possibilities to reduce the computational complexity of the algorithm in NLoS conditions. For example, the exhaustive search could be replaced with random sampling [17] if the number of measurements would be really high so that the exhaustive search would become prohibitive. In addition, the grid search over the angles could be implemented using a coarse grid in combination with a gradient-based optimization method [12]. These two alternatives are two good candidate solutions to improve efficiency of the proposed algorithm in future research.

## V. Conclusion

The paper presented a robust radio SLAM algorithm for mixed LoS/NLoS environments that can estimate the unknown UE state, incidence point of single-bounce propagation paths, as well as existence of the LoS path, using measurements that are corrupted by outliers. Analysis was carried out using experimental mmWave measurements and the results demonstrated the importance of detecting the outliers and existence of the LoS. The newly proposed radio SLAM algorithm admits numerous possibilities of future research into other mmWave localization and sensing approaches or enhancements via filtering and smoothing.

## References


[1] A. Behravan et al., "Positioning and sensing in 6G: Gaps, challenges, and opportunities," *IEEE Veh. Technol. Mag.*, vol. 18, no. 1, pp. 40–48, Mar. 2023.

[2] C. De Lima et al., "Convergent communication, sensing and localization in 6G systems: An overview of technologies, opportunities and challenges," *IEEE Access*, vol. 9, pp. 26902–26925, 2021.

[3] X. Liu, Z. Cao, Y. Yu, G. Ren, J. Yu, and M. Tan, "Robot navigation based on situational awareness," *IEEE Trans. Cogn. Devlop. Syst.*, vol. 14, no. 3, pp. 869–881, Sep. 2022.

[4] C. B. Barneto et al., "Millimeter-wave mobile sensing and environment mapping: Models, algorithms and validation," *IEEE Trans. Veh. Technol.*, vol. 71, no. 4, pp. 3900–3916, Apr. 2022.

[5] A. Shahmansoori, G. E. Garcia, G. Destino, G. Seco-Granados, and H. Wymeersch, "Position and orientation estimation through millimeter-wave MIMO in 5G systems," *IEEE Trans. Wireless Commun.*, vol. 17, no. 3, pp. 1822–1835, Mar. 2018.

[6] H. Wymeersch et al., "5G mm wave downlink vehicular positioning," in *Proc. IEEE Glob. Commun. Conf.*, 2018, pp. 206–212.

[7] F. Wen and H. Wymeersch, "5G synchronization, positioning, and mapping from diffuse multipath," *IEEE Wireless Commun. Lett.*, vol. 10, no. 1, pp. 43–47, Jan. 2021.

[8] Y. Ge et al., "A computationally efficient EK-PMBM filter for bistatic mmWave radio SLAM," *IEEE J. Sel. Areas Commun.*, vol. 40, no. 7, pp. 2179–2192, Jul. 2022.

[9] H. Kim, K. Granström, L. Gao, G. Battistelli, S. Kim, and H. Wymeersch, "5G mmWave cooperative positioning and mapping using multi-model PHD filter and map fusion," *IEEE Trans. Wireless Commun.*, vol. 19, no. 6, pp. 3782–3795, Jun. 2020.

[10] O. Kaltiokallio et al., "Towards real-time radio-SLAM via optimal importance sampling," in *Proc. IEEE 23rd Int. Workshop Signal Process. Adv. Wireless Commun.*, 2022, pp. 1–5.

[11] Y. Ge et al., "Experimental validation of single BS 5G mmWave positioning and mapping for intelligent transport," *IEEE Trans. Veh. Technol.*, vol. 73, no. 11, pp. 16744–16757, Nov. 2024.

[12] M. A. Nazari, G. Seco-Granados, P. Johannisson, and H. Wymeersch, "mmWave 6D radio localization with a snapshot observation from a single BS," *IEEE Trans. Veh. Technol.*, vol. 72, no. 7, pp. 8914–8928, Jul. 2023.

[13] E. Rastorgueva-Foi et al., "Millimeter-wave radio SLAM: End-to-end processing methods and experimental validation," *IEEE J. Sel. Areas Commun.*, vol. 42, no. 9, pp. 2550–2567, Sep. 2024.

[14] X. Cheng, C. Tang, and Z. Zhang, "Accurate channel estimation for millimeter-wave MIMO systems," *IEEE Trans. Veh. Technol.*, vol. 68, no. 5, pp. 5159–5163, May 2019.

[15] R. Mendrzik, H. Wymeersch, G. Bauch, and Z. Abu-Shaban, "Harnessing NLOS components for position and orientation estimation in 5G millimeter wave MIMO," *IEEE Trans. Wireless Commun.*, vol. 18, no. 1, pp. 93–107, Jan. 2019.

[16] S. Boyd and L. Vandenberghe, *Convex Optimization*. Cambridge, U.K.: Cambridge Univ. Press, 2004.

[17] M. A. Fischler and R. C. Bolles, "Random sample consensus: A paradigm for model fitting with applications to image analysis and automated cartography," *Commun. ACM*, vol. 24, no. 6, pp. 381–395, Jun. 1981.

[18] C. Gustafson, K. Haneda, S. Wyne, and F. Tufvesson, "On mm-wave multipath clustering and channel modeling," *IEEE Trans. Antennas Propag.*, vol. 62, no. 3, pp. 1445–1455, Mar. 2014.

[19] Q. Bader, S. Saleh, M. Elhabiby, and A. Noureldin, "NLoS detection for enhanced 5G mmWave-based positioning for vehicular IoT applications," in *Proc. IEEE Glob. Commun. Conf.*, 2022, pp. 5643–5648.

[20] I. Güvenç et al., "NLOS identification and weighted least-squares localization for UWB systems using multipath channel statistics," *EURASIP J. Adv. Signal Process.*, vol. 2008, Jan. 2008, Art. no. 271984.

[21] P. F. M. Smulders, "Statistical characterization of 60-GHz indoor radio channels," *IEEE Trans. Antennas Propag.*, vol. 57, no. 10, pp. 2820–2829, Oct. 2009.

[22] E. Rastorgueva-Foi et al., "Millimeter-wave radio SLAM: 60 GHz indoor sensing dataset," IEEE Dataport, 2024, doi: 10.21227/xskh-dk87.